Experimental Study of a Turbulent Cross-Flow Near a Two-Dimensional Rough Wall with Narrow Apertures

Satya Mokamati and James A. Olson
The Pulp and Paper Centre, University of British Columbia, Vancouver, Canada, and
Dept. of Mechanical Engineering, University of British Columbia, Vancouver, Canada

D. Mark Martinez
The Pulp and Paper Centre, University of British Columbia, Vancouver, Canada, and
Dept. of Chemical and Biological Engineering, University of British Columbia, Vancouver, Canada

Robert W. Gooding
Advanced Fibre Technologies, Montreal, Canada

DOI 10.1002/aic.11575
Published online July 22, 2008 in Wiley InterScience (www.interscience.wiley.com).

Turbulent flow over a rough wall with suction or blowing is a common fluid mechanics problem that has many practical applications including pulp screening. To better understand, the complex hydrodynamics at the critical region near the surface of the wall, the streamwise mean and velocity fluctuations were determined experimentally using laser Doppler velocietry. The near-wall streamwise velocity fluctuations and local mean streamwise velocity were shown to be a strong function of the surface roughness, and the aperture and cross-flow velocities. A correlation for the mean velocity and the wall shear stress acting near the wall was determined. © 2008 American Institute of Chemical Engineers *AIChE J,* 54: 2516–2526, 2008
Keywords: pulp screening, surface roughness, laser Doppler anemometer, roughness function, turbulence, near-wall, suction

Introduction

In this work, we consider the turbulent cross-flow of a Newtonian fluid in a channel with a contoured, slotted lower boundary undergoing suction (see Figure 1). The two-dimensional roughness of the channel lower wall is formed by transversely placing the roughness elements in a test coupon to the approaching flow. The test coupon is made from the contoured wires banded together to form a regularly spaced array of 2D roughness elements with narrow slots. The motivation for the present investigation stems from an interest in the screening of papermaking fiber suspensions. In this application, a fiber suspension enters a pulp screen and passes into an annular space between a slotted, stationary outer cylinder and a rotor as shown in Figure 2. The rotor induces a tangential or cross-flow velocity in the order of 10–20 m/s and is equipped with protruding elements that periodically back-flush the apertures in the cylinder.[1] The apertures in the cylinder are typically slots with widths in the range of 0.1–0.2 mm. Papermaking fibers are 1–3 mm long and 20–40 microns in diameter.[2] Screened fibers pass through the apertures while the oversized contaminants are retained in the annular space and pass out of a reject port. In addition to the tangential flow (or cross-flow), the axial velocity is in the

Correspondence concerning this article should be addressed to J. A. Olson at olson@mech.ubc.ca.

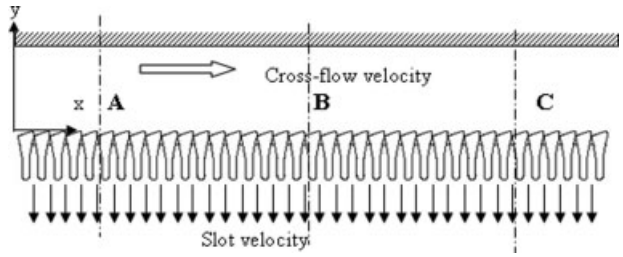

Figure 1. Flow geometry considered.

order of 0.5 m/s. The time-averaged velocity through a slot is typically in the range from 1 to 5 m/s. Pulp screening improves paper properties through the removal of oversized contaminants, such as fiber bundles, plastic, metal, and other debris. In addition to the contaminant removal, screens are sometimes used to upgrade the pulp quality by separating the fibers into different fractions for targeted processing.

The screen cylinder is thus one of the two critical components of a pulp screen, with the other being the rotor. The performance of the screen is dependent on the geometry of the aperture. The cylinder has apertures which may be either holes or slots. Slotted screens are typically manufactured from bars or wires that have a cross-section that is approximately triangular. As shown in Figure 1, these wires are banded into a regularly-spaced array with their long axes parallel to each other. In cross-section, the banded wires are ~2–4 mm wide, 10 mm high, and separated by a gap of 0.1–0.2 mm (which defines the slot width), as shown in Figure 3. The dimensions and spacing of the wires are closely related to the macroscopic roughness of the cylinder surface. The cross-sectional shape of the wire defines a "contour" on the inlet side of the screen cylinder. The shape of the contour is intended to provide three effects: (i) to fluidize the pulp suspension by the dissipation of turbulent energy, (ii) to reduce the hydraulic resistance of the flow in the slot, and (iii) to promote the passage of fibres through the slot.

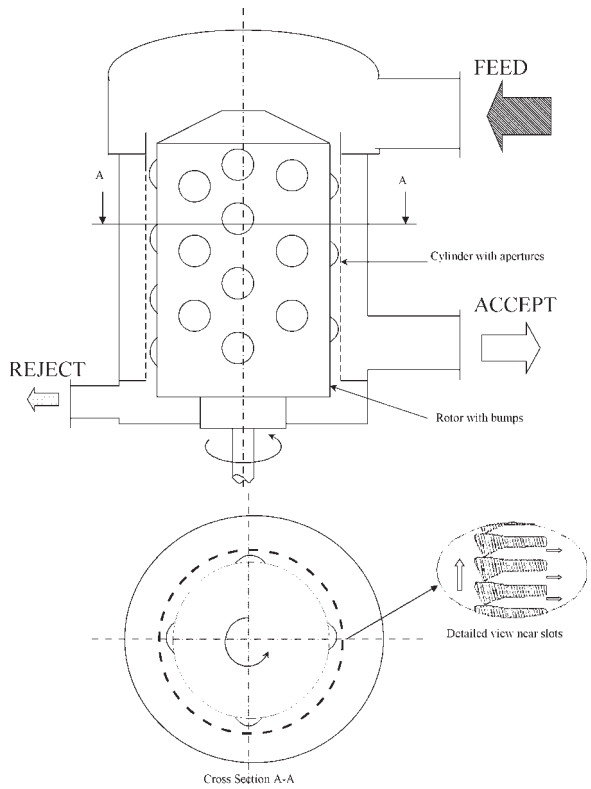

Figure 2. Schematic of the principal flows through a pressure screen.

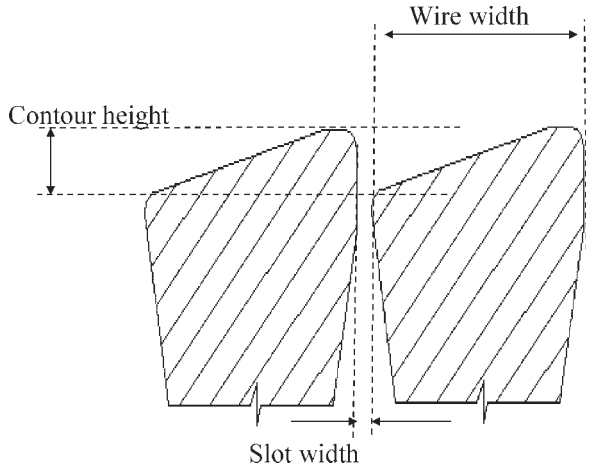

Figure 3. Close-up of the wire cross-section near the feed surface showing wire width, slot width, and contour height.

Optimal design of screening systems requires a range of wire heights and widths to ensure an appropriate compromise between capacity (throughput) and contaminant removal efficiency. Previous studies[3–7] show that the cross-flow and slot velocities, and wire shape dramatically affect the flow field near the wall. This, in turn, controls the fiber and contaminant passage through the apertures and the overall performance of the screen. Gooding[4] showed that the screen apertures with contours reduce hydraulic resistance, and that the velocity patterns at the slot entry are determined by the contour shape. The presence of contours increase the turbulence near the screen cylinder surface when compared to a screen cylinder without contours.[4,7,8] Halonen and Ljokkoi,[8] for example, observed a 15% increase in the turbulent intensity when a contour was present in the screen cylinder design. The increased turbulence results in more mixing near the surface and enhances the passage of the long fibers through the slots, increasing the pulp concentration in the accept stream and the mass flow rate through the screen.[9]

Insight into the behavior of screens can be obtained by examining a number of related studies which reflect aspects of the screen flow considered here. In the first category of flows to consider are laminar boundary layers over a smooth flat plate with the uniform suction. This case has been summarized in a number of classic texts, see for example White[10] and the references contained therein, and the cross-flow velocity is given by an Eq. 1 of the form

$$u = U_\infty(1 - \exp(vy/v);\ v(x,y) = V_w < 0 \qquad (1)$$

where u is the local cross-flow velocity; v is the velocity normal to the flat plate; y is the normal distance from plate, v is

the kinematic viscosity; and V_w is the suction velocity. It is worth noting that this simple relationship is an exact solution of the Navier-Stokes equations.

As discussed earlier, due to the large tangential velocity, laminar flow conditions do not exist in the pulp screen. In addition, the flow through the slot is a complex transitional flow. Also, we need to clarify terminology used to represent the flow through the lower boundary, that is, a clear definition is required to distinguish slot velocity and suction velocity. The slot velocity, V_s, is the average intrinsic velocity in the slot whereas the suction velocity, V_w, is superficial or seepage velocity through the screen wall. The two are related by the following:

$$V_w = \frac{s}{s+w} V_s \tag{2}$$

where s is slot width, and w is wire width. For a slot width of 0.15 mm and wire width of 3.2 mm the suction velocity is approximately twenty-two times less than the slot velocity.

Flow over smooth surfaces with the suction or blowing has been studied in great detail by the aeronautics community for boundary layer control, with most of the work focused on skin friction reduction. Typically, the drag is reduced by utilizing wall suction through an array of small circular holes drilled in the wing surface to reduce the boundary layer. This is similar to the flow near the surface of the screen cylinder in a pressure screen, where the rotor induces a cross-flow which is pulled through the drilled or slotted apertures. As described earlier, the entry of the screen aperture can be either smooth or contoured to improve the fiber passage and to reduce the hydraulic resistance. Therefore, the flow of interest to this investigation generally resembles the case of flow over a rough surface with suction.

Thomas and Cornelius[11] examined the suction of a laminar boundary layer into a slot in a smooth wall. They observed a vortex bubble in the slot and the size of this bubble increased with increasing cross-flow velocity or reduced slot velocity. They also noted that the slot resistance increased due to the presence of stationary vortices in the slot. Sano and Hirayama[12] examined the effect of steady suction or blowing through a span-wise slit in a turbulent boundary layer. They found that as the suction velocity decreased, the skin friction and turbulence intensity behind the slit also decreased. Antonia et al.[13] demonstrated that the turbulent boundary layer can be relaminarized by an intensive local suction with the skin friction being reduced during the relaminarization. In this study, the suction effect is applied through a short porous wall strip. Yoshioka et al.[14] performed an experimental investigation of free stream turbulence-induced disturbances in the boundary layers with the wall suction. The experiments showed that the wall suction suppresses the disturbances' growth and significantly delays or inhibits the breakdown to turbulence.

In the case most relevant to our work, we find that the properties of a flow field over a rough surface have been studied experimentally since the early work of Nikuradse,[15] which focused on densely-packed, uniform sand grain roughness. With a turbulent boundary layer over a smooth plate without suction, Nikuradse[15] gives the following relation for the velocity in the over-lap region of the wall:

$$u^+ = \frac{1}{\kappa}\ln(y^+) + B \tag{3}$$

where u^+ is the dimensionless cross-flow defined by $u\sqrt{\rho/\tau_w}$; y^+ is the dimensionless distance normal to the wall defined by $y\sqrt{\tau_w/\rho}/\nu$; κ is the von Karman constant and B is an additive constant; and ρ and ν are the fluid density and kinematic viscosity, respectively. It is common to find different κ and B in the literature, for example, κ variations of $0.38 < \kappa < 0.45$ and B variations of $3.5 < B < 6.1$.[16] However, in this study we considered $\kappa = 0.421$ and $B = 5.6$ which were suggested by Shockling et al.[17] The presence of roughness displaces the velocity profiles downwards so that

$$u^+ = \frac{1}{\kappa}\ln(y^+) + B - \Delta B(k_s^+) \tag{4}$$

where k_s^+ is a roughness Reynolds number defined by $k_s\sqrt{\tau_w/\rho}/\nu$. The roughness function, ΔB, depends on type of roughness such as sand, sand mixture, threads, spheres etc. Correlations between skin friction and roughness type were established from these investigations.

The roughness is represented by roughness height, k_s, however the geometry considered in the present study has two length scales (contour height, h and wire width, w). In k-type roughness (rough walls with grooves wider than four times roughness height), the roughness height alone is not sufficient to characterize the wall roughness,[18] and several attempts have been made to express the roughness in terms of other parameters. Simpson[19] defined a roughness density as the ratio of the total surface area to the total roughness frontal area normal to the flow direction. In the present study, the screen geometry falls between k-type and d-type roughness. The roughness function in this study is represented by both the length scales (h and w) and not just by roughness (contour) height (h).

For flow over a rough wall with the suction or blowing, the stream-wise velocity profile changes significantly and the law of the wall needs to be modified to accommodate the suction or blowing. Schlichting[20] conducted studies on the suction and blowing effects on the boundary layer under zero pressure gradients. Stevenson[21] and Schlichting[20] derived the following modification of the logarithmic law of the wall where either the suction or blowing is present:

$$\frac{2}{V_w^+}\left[\left(1 + V_w^+ u^+\right)^{1/2} - 1\right] \approx \frac{1}{\kappa}\ln(y^+) + B \tag{5}$$

Equation 5 reduces to Eq. 3 in the limit of $V_w^+ \to 0$. This result is obtained through the use of L'Hôpital's rule.

The roughness function, ΔB, depends on the size and the type of roughness and the effective location of the fictitious wall from which the distance is measured.[22] In near-rough wall modeling with Computational Fluid Dynamics (CFD), the surface roughness is taken into account through the introduction of the surface roughness length scale k_s^+ and the roughness function ΔB in the log-law of the wall.[23] The near-wall treatment with a modified log-law is used instead of solving the detailed flow over rough surface in order to save computational time and resources. Gregoire et al.[24] modeled the flow field near the wall of a pulp screen using

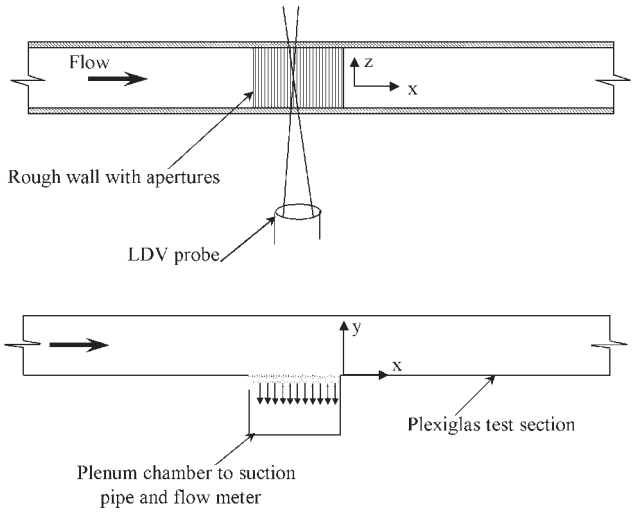

Figure 4. Schematic of the experimental system.

CFD by implementing a modified log-law for the near-wall treatment. The log-law was modified using a roughness function determined for the sand grains found in the literature. The concept of equivalent sand grain roughness for a wire contour height may not be the best approximation, as the sand grains do not represent the complex details of the contour geometry. This article focuses on determining the roughness functions for a range of the industrial contour geometries.

In this work, we used Laser Doppler Velocietry (LDV) to examine how the cross-flow and slot velocities, contour height and wire width affect the details of the fluid flow near a periodic array of wires, which represent the cross-section of a screen cylinder. In this study, we measure the streamwise mean and fluctuating velocity profiles, and develop a correlation for ΔB as a function of mean streamwise velocity, suction velocity, contour height, and wire width. In the context of this study, "mean streamwise velocity" refers to a local cross-flow velocity, which is averaged over time, but varies according to the distance away from the rough wall.

Experimental System

Flow channel and flow loop

The experiments were carried out on a flow channel as shown in Figure 4. The channel was intended to simulate the flow through a section of the screen cylinder under steady flow conditions after making the following simplifications and assumptions. In studying the flow at the screen surface in a pulp screen (see Figure 2), the variations in the axial screen flow are secondary compared to tangential flow (cross-flow) induced by the rotor and also the flow is periodic between rotor elements. Therefore, based on these assumptions, a three-dimensional pulp screen cylinder flow can be reduced to flow over a periodic array of wires. The problem can be further simplified by assuming that the unsteady phenomena associated with the rotor pulsations are localized during the passage of the hydrodynamic elements and may be disregarded during the rest of the time. With that simplification, we can neglect the presence of rotor and the pressure pulses produced by the rotor. As a result, the test coupon (flush-mounted horizontally inside of the channel) used in the present study resembles the flow over a periodic array of wires under steady cross-flow conditions. In addition to the above simplifications, we considered water as the working fluid. The low consistency pulp suspensions (<1%) have the same flow properties as water in a fully turbulent state.[25] Therefore, the insights gained from water as the working medium can be related to the low consistency pulp suspension used in an industrial screen. The flow channel used in this study is made from Plexiglas with 12.5 mm wall thickness. The channel is 1244 mm long and has 38.1 mm $\times$ 38.1 mm square cross-section. The flow is from the left to right of the channel as shown in Figure 4 and the upstream flow passes through the slots on the lower boundary and enters the plenum. This apparatus is very similar to those used by Gooding,[3,4] Kumar,[5] and Olson[6] to observe the fiber motion near an aperture.

The primary component of the experimental system is the test coupon. All the test coupons were 152.4 mm long and 38.1 mm wide. Five coupons with different geometries were tested (Table 1). The geometry of the slots used in this study was taken from the commercial pulp screens. The coupons were made from commercial, stainless steel, wires. The design of the flow channel is modular so that the test coupons can be flush-mounted horizontally inside of the channel and can be replaced very quickly and easily.

The flow loop was comprised of a circulation pump, two magnetic flow meters, a 0.2 m^3 tank, and the flow channel. In an industrial pulp screen, the cross-flow velocities are in the order of 10–20 m/s and the slot velocities are in the order of 0.8–5.0 m/s. Because of the limited capacity of the pump, only 10 m/s average cross-flow velocity could be achieved in a 38 $\times$ 38 mm square channel. The flow rate was controlled by a pump with a variable frequency drive. The pump has a 28 kW motor and was connected to the flow channel with 76 mm diameter schedule 80 PVC pipe. The flow from the channel was diverted back to the tank. The flow from the plenum at the bottom of the coupon was also diverted back to the tank with 25 mm diameter schedule 80 PVC pipe. Flow through the test coupon was set within a range from 0.25 to 10 m/s using a ball valve. The cross-flow velocity was measured using a 76 mm diameter magnetic flow meter (Rosemount 8712D series) and the volumetric flow rate through the test coupon was measured with a 25 mm diameter magnetic flow meter (Rosemount 8712D series).

Table 1. Experimental Variables for LDV Measurements

Working Fluid				Water
Upstream Velocity				10 m/s
Slot Velocity				0.25–10 m/s
Dimensions of Test Coupons	Coupon #	Contour Height (mm)	Wire Width (mm)	Slot Width (mm)
	1	1.2	3.2	0.15
	2	0.9	3.2	0.15
	3	0.6	3.2	0.15
	4	0.6	2.6	0.15
	5	0.9	4.0	0.15

LDV measurements

A commercially available fiber optic LDV system was used to record the mean velocities and rms velocity fluctuations. The mean velocity refers to the average velocity value of all the velocities measured at a particular point. Thus,

$$u = \frac{\sum_{i=1}^{n} (\mathbf{u}.e1)_i}{n} \tag{6}$$

where u is the average velocity at a point, $\mathbf{u}$ is the velocity for the i^{th} seeding particle, and n is the number of particles measured (or the number of samples taken per point). The root mean square (rms) fluctuating velocity, which is also the standard deviation of the velocities measured, is given as

$$\sqrt{\overline{u'^2}} = \sqrt{\frac{\sum_{i=1}^{n} (\mathbf{u}.e1 - u)_i^2}{n-1}} \tag{7}$$

where $\sqrt{\overline{u'^2}}$ is the streamwise rms fluctuating velocity.

The principle of this measurement technique has been described in detail in Durst et al.[26] The LDV used in this study was a single-component dual-beam system in back scatter mode. Only one-dimensional measurements (streamwise) were performed in the experiments. The LDV probe is mounted on an automated two axis traverse unit, which is controlled by the data acquisition software. The origin for taking measurements on the wall is defined as the plane where the probe measurement volume just touches the coupon top surface. This was done by moving the probe measurement volume closer and closer to the wall until LDV no longer detected any Doppler bursts. There is no data in the contours due to the blockage of the laser beams by the contours of the coupon. The flow was seeded with 100 nm Titanium Dioxide (TiO_2) particles.

For each run, the flow in the channel was established, and LDV system was activated. Band pass filters were adjusted until a strong burst signal was found. Start and end positions of the velocity profile and the number of data points along that profile was specified. When the acquisition started, the traverse moved to the next position automatically where the next set of measurements were taken. The data acquisition software would optimize the velocity profile data recording and adapt the filter settings and data acquisition for each data point. The system was needed to be set up for the first point only. In this manner, the system was able to make the complete survey without the user intervention. At every data point of the profile, the raw data along with the information about the mean (Eq. 6) and rms fluctuating (Eq.7) velocity was recorded. The number of samples required to achieve statistically independent results depend on the local streamwise rms velocity fluctuations. It was found that at least 100 samples were required for each data point in the profile to be 95% certain that rms velocity fluctuations were within 5% of true rms value.

Uncertainties in the LDV measurements are dependent on the accuracy of the LDV system, the accuracy in locating the measurement plane and the statistical uncertainty of the measurements. The accuracy of the LDV system specified by the manufacturer is ± 8 mm/s. The 90% confidence interval for the mean velocity was calculated using the student's t-distribution. The maximum uncertainty in the mean velocity near the wall is estimated to be $\pm$ 7% and away from the wall in the free stream is $\pm$ 5%. The estimated maximum fractional uncertainty in the RMS velocity is $\pm$ 12%. The error in accurately locating the measurement plane is estimated to be $\pm$ 0.1 mm (half the size of the measurement volume). Accuracy of the traverse system is $\pm$ 0.01 mm. Therefore, total error in locating the y-ordinate is at most, $y^+ \leq \pm 16.65$ (± 0.11 mm).

The effect of channel geometry and measurement location

The entry to the channel was an abrupt contraction from a circular pipe of 76 mm diameter. The entry length could be estimated from similar flows reported in the literature. Lissenburg et al.[27] investigated the effect of a constriction on turbulent pipe flow with Reynolds number is equal to 5000. They found that, after 10 pipe diameter distance downstream from the constriction an almost complete recovery of the disturbed turbulent flow was obtained. Even shorter distances were found for higher Reynolds numbers.[28] In our channel, the slotted boundary (called the test coupon) was located at 14 equivalent diameters from the channel entry. All the measurements were made in the centre plane at half the width ($\approx$19 mm) of the channel. The measurements were made from the top of the roughness elements. However, the virtual origin is located below the top of the roughness elements (roughness varied from 0.6 to 1.2 mm), such that the vertical distance from wall, $y = y' + h$. The Reynolds number of the flow in the channel, based on the equivalent diameter of the channel and the cross-flow velocity, is $\sim$546,000 (kinematic viscosity is taken as 0.6966×10^6 at 37°C).

In order to test the reliability of the experimental system, measurements were performed over the impermeable smooth wall (from top wall at location B shown in Figure 1) to validate the data with well-established experimental data. The measurements were compared with logarithmic law of the wall for a smooth impermeable wall. Figure 5 shows that the measured profile follows the log-law within 5%. The data is best fitted to the log-law line obtained using Shockling's et al. 's[17] constants compared to Coles' and Hirst's constants.[29] The shear velocity is determined using curve fitting technique similar to the procedure outlined in the later sections. Although for a smooth wall boundary layer, u^* can be easily determined, it is less straight forward for a rough wall where the wall shear stress receives contributions from the form drag and viscous shear stress. In the case of rough wall, it is more complicated to calculate the shear stress because the velocity profile is affected by the roughness through additional variable in the log-law, the roughness function ΔB (or Δu^+, a shift in the velocity profile with respect to that of a smooth wall). It is not always possible to determine u^* from direct wall shear stress measurements. Although a number of indirect techniques are available for determining u^*, none are universally accepted. Among them is the Clauser chart method, which is widely used to determine u^*. This method masks the subtle Reynolds-number-dependent behavior in the wall region.[30] Kendall and Koochesfahani[31] proposed a

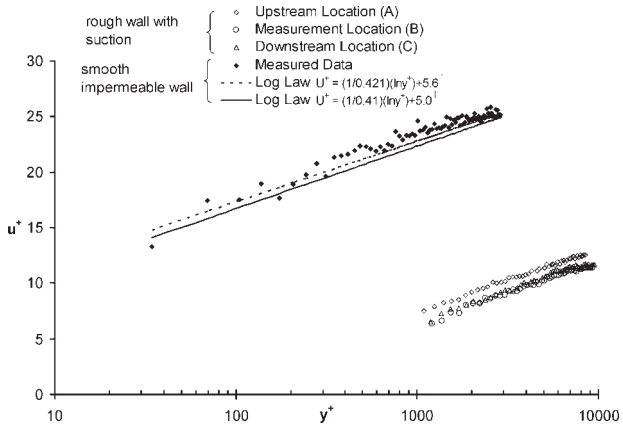

Figure 5. Comparison of experimental velocity profiles for a smooth wall with classical log-law of the wall (†Shockling's et al. 's[17] constants; ††Coles' and Hirst's constants[29]) and sensitivity of measurements along the rough wall with suction.

method to estimate the shear velocity by fitting the smooth wall data to the Spalding[32] profile. The Spalding profile approximates the mean velocity profile of a smooth wall using a power-series scheme joining the linear sub-layer to the logarithmic region. The shear velocity is estimated for the smooth impermeable wall by fitting its data to Spalding profile using the procedure outlined in Kendall and Kooches-fahani.[31] In comparison, the method used in this study under estimated the shear velocity for the smooth impermeable wall by 4.8%.

The boundary layer thickness of the velocity profile measured from the top wall is ~4 mm, which indicates that the velocity gradient and the Reynolds stresses must be zero at the centerline which is 19.05 mm (y^+ = 10,646.6) away from the wall. It clearly states that, at the Reynolds number (Re = 546, 000) investigated in this study, the dimensionless channel half-width is 10,646 viscous lengths which places the channel centerline far away from the outer layer of all four sides of the wall. Therefore, we can ignore the side wall effects on the measurements taken at the center plane of the channel.

The sensitivity of the measurements along the length of the coupon is also tested by comparing the velocity profiles at three different positions as shown in Figure 1. All the measurements in this study were taken at location B. Two other locations were chosen for comparative purposes—location A is chosen 12 slots upstream of B and location C is chosen 12 slots downstream of B. For all the three locations the measurements were taken immediately downstream of each slot. Figure 5 shows that the profiles associated with location B and location C collapse on to a single curve. However, the velocity profile at location A is off-set by 5% compared to the other two locations. This difference might have been attributed due to the tripping of boundary layer caused by the roughness elements (wire contours). As shown in Figure 4, the test coupon was flush mounted in the middle of the channel, which has smooth flat surface. The flow approaching the test coupon experiences an abrupt change in the surface texture from an impermeable smooth surface to rough porous surface. The collapse of the two curves at location B and C indicates that the flow has fully-developed over the coupon at the measurement location.

Results and Discussion

Experiments were performed with five different test coupons to measure the mean and fluctuating streamwise velocity profiles. The experimental results obtained for the five coupons can be broadly grouped into two categories: (1) the effect of wire geometry characterized by contour height and wire width, and (2) the effect of slot velocity. In the first category of experiments, the slot velocity and cross-flow velocity were kept constant: V_s = 1 m/s, U_∞ = 10 m/s. In the second category, the cross-flow velocity was kept constant at U_∞ = 10 m/s and the slot velocity was varied between 0.25 m/s and 10 m/s.

Figure 6 shows the mean velocity distribution for all the wire geometries plotted on a semi-log plot. All the wire geometries displayed a linear log region that is similar to the velocity profile above a smooth wall (not shown in the graph) but shifted downwards. The semi-logarithmic velocity distribution curve is shifted downwards by an amount Δu^+ depending on the contour slope (h/w), showing that Δu^+ is a function of contour height and wire width. The figure shows that the over-lap region extends to $y^+ > 900$ because of high Reynolds number flow ($Re = 5.5 \times 10^5$) and fully rough wall ($k_s^+ > 516$). The extent of the logarithmic layer moves to larger values of y^+ for higher contours. For a smooth impermeable wall, the over-lap region is between y^+ equal to 35 and 350.[10] Shockling et al.[17] and Bakkena et al.[33] also found over-lap region with $y^+ > 1000$ for high Reynolds number flow ($> 5 \times 10^5$) and fully rough wall regions As shown in Figure 6, the mean velocity decreased with increasing contour height and increased with increasing wire width. As the contour height increases the flow becomes rougher. This is due to the increase in the protrusion of the contours into the flow in the vicinity of the wall. These contours act as blockages to the flow adjacent to the wall. As the contour

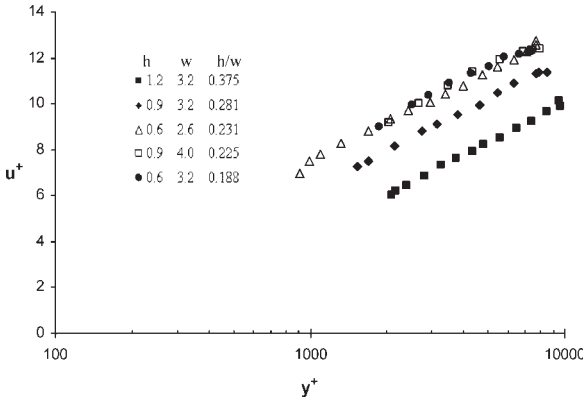

Figure 6. Mean velocity profiles for boundary layers with V_s = 1 m/s and U_∞ = 10 m/s for different contour heights and wire widths.

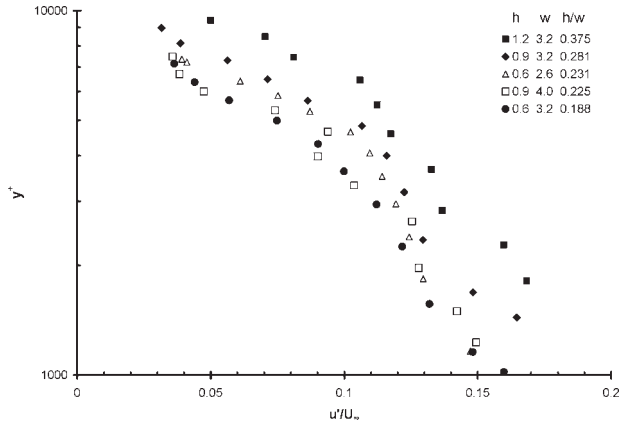

Figure 7. Variation of stream-wise velocity fluctuations for different contour heights and wire widths in wall coordinates at $U_\infty = 10$ m/s and $V_s = 1$ m/s.

height increases, the intensity of vortex shedding process above the viscous layer increases, leading to the gradual destruction of this layer and an increase in the skin friction drag. The velocity profiles for wire geometries with similar contour height to wire width ratios that are nearly the same, that is: $h = 0.6$, $w = 2.6$, ($h/w = 0.231$); $h = 0.9$, $w = 4.0$, ($h/w = 0.225$); $h = 0.6$, $w = 3.2$, ($h/w = 0.188$). The increased roughness due to narrower wire widths (contours per unit length of screen surface) also decreases the local velocity near the screen surface, which is quite significant for $h = 0.9$, $w = 3.2$ when compared with $h = 0.9$, $w = 4.0$.

Figure 7 shows the stream-wise velocity fluctuations measured for all five wire geometries at 1 m/s slot velocity. The stream-wise velocity fluctuations are nondimesionalized with respect to average free stream velocity (U_∞) and plotted against y^+. Nondimensionalization by the free stream velocity describes the intensity of the velocity fluctuations relative to the square root of the mean turbulent kinetic energy at a given distance from wall. Also, the overall effect of the wire geometry can be illustrated by scaling the streamwise velocity fluctuations data with the free stream velocity. From Figure 7, it is observed that the effect of wire geometry is much more pronounced when streamwise velocity fluctuations are scaled with the free stream velocity. The roughness effect produced by the contours with similar geometry (i.e. shallower contour slope) on the streamwise velocity fluctuations is similar. This figure also shows that the ratio of stream-wise velocity fluctuations to the mean free stream velocity decrease with distance away from the wall from about 0.15 near the wall to a level of ~0.04. The maximum stream-wise velocity fluctuations (≈0.15) near the wall corresponds to a 1.5 m/s fluctuating component of x-velocity (u') which is less than 1% agreement with the LDV measurements done by Halonen and Ljokkoi[8] over a contoured screen coupon. The stream-wise velocity fluctuations measurements were available only above $y^+ \approx 900$ because it was not possible to get the LDV data very close to the wall. Furthermore, the figure shows that the stream-wise velocity fluctuations increase with increasing contour height and decreasing wire width. As wire width decreases, the apparent roughness of the surface increases (the number of contours per unit length) which is thought to be responsible for the increase in stream-wise velocity fluctuations. Also, the denser contour geometry would promote a greater flow interaction between the contours (or roughness elements). Low contour heights and wider wires constitute shallower sloped contours, which gave higher local velocities and lower streamwise fluctuation levels near the wall compared to higher sloped contours.

Figure 8 shows the mean velocity profiles for all the geometries at varying slot velocities and a constant cross-flow velocity. For all geometries, the velocity profile is approximately log-linear and u^+ increases with slot velocity. The increase in the mean velocity is due to the reduction in boundary layer height with increasing the slot velocity, that is, high velocity flow is pulled closer to the screen surface as more fluid is pulled through the apertures. At low slot velocities, the differences in the shear velocity are very small when compared with that at high slot velocities.

It is unclear how the increase in upstream velocity with increased slot velocity affects screen performance—though it has been hypothesized that the increasing local upstream velocity increases contaminant removal and fractionation.[9] Slot velocity, however, is recognized as a critical factor affecting the screen performance for certain industrial applications where the passage of contaminants is limited by factors other than simple mechanical interference. For these applications, the efficiency of the screen decreases at high slot velocities. Fiber passage will also increase with increased slot velocity, which leads to an increase in screen accept concentration.[9]

Figure 9 shows the stream-wise velocity fluctuations above the screen surface for all the geometries at various slot velocities and a constant cross-flow velocity of 10 m/s. The stream-wise velocity fluctuations are a maximum near the wall and decrease to a level of ~0.04. The near-wall stream-wise velocity fluctuations decrease with increased suction rate, as the turbulent kinetic energy is convected from the screen surface through the apertures. The decrease in stream-wise velocity fluctuations at high slot velocities may affect the ability of the contours to break up any fiber flocs above the screen.

The mean velocity profiles obtained for five test coupons at various slot velocities can be used to obtain a roughness function, ΔB. In the present study, the shear velocity required to calculate ΔB is determined by fitting the experimental data in the following way. The logarithmic law is modified from its original form to include the effects of both the dimensions of contour (h and w) as well as slot velocity with $\Delta B(h, w, V_s)$ so that,

$$u^+ = \frac{1}{\kappa}\ln\,(y^+) + B - \Delta B(h, w, V_s) \tag{8}$$

The last two terms in Eq. 8 are combined so that,

$$u^+ = \frac{1}{\kappa}\ln\,(y^+) - \frac{1}{\kappa}\ln\,(C^+) \tag{9}$$

where $-\frac{1}{\kappa}\ln\,(C^+) = B - \Delta B(h, w, V_s) = -B'$ Here, we grouped B and ΔB together to define a new log-law constant B' given by, $B' = -B + \Delta B(h, w, V_s)$

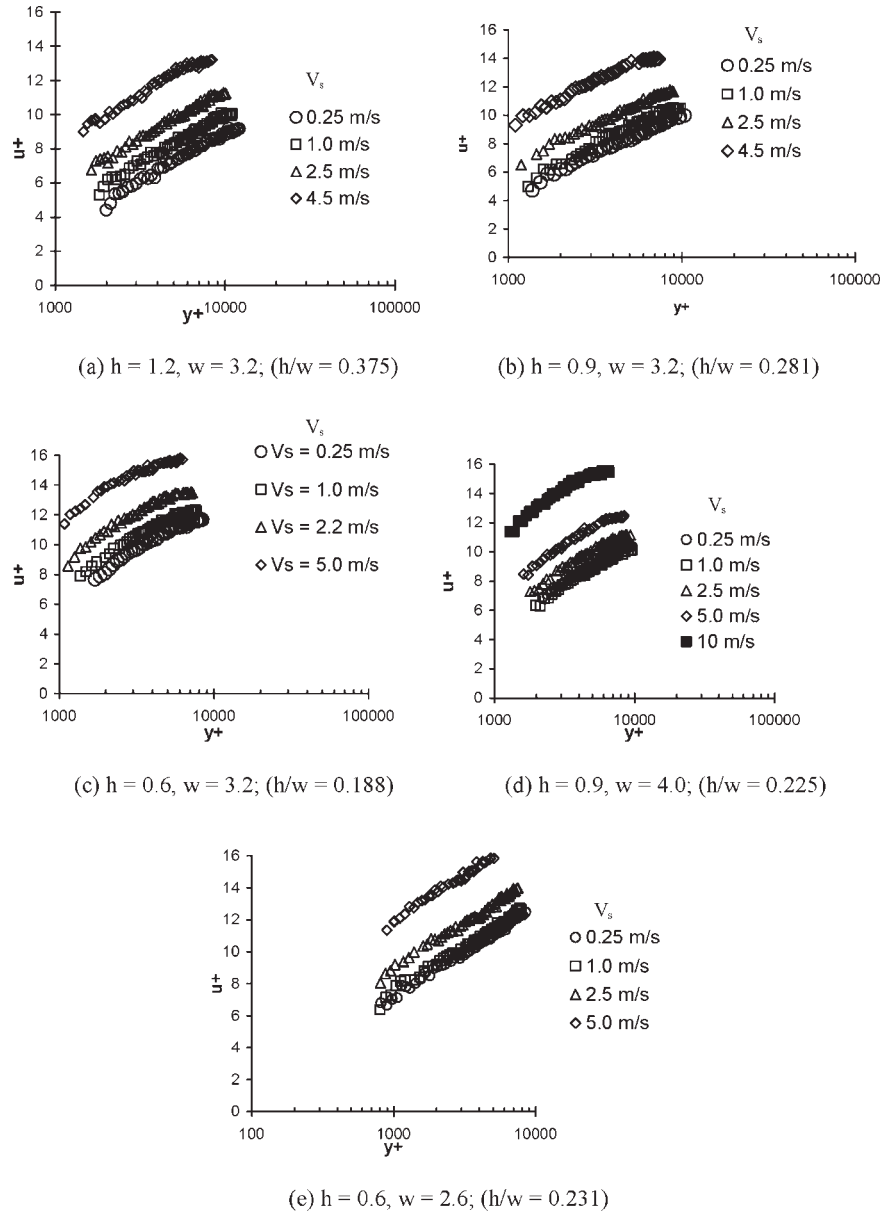

Figure 8. Effect of wall suction on the wall normal distribution of the mean velocity profiles.

Now the Eq. 8 becomes,

$$u = \frac{u^*}{\kappa}\ln\left(\frac{y}{C}\right) \quad \text{or}$$
$$u = \frac{u^*}{\kappa}\ln(y) \; - \; \frac{u^*}{\kappa}\ln(C) \tag{10}$$

When the experimental data of the each mean-velocity profile is fitted with a linear regression and matched with Eq. 10, the slope of the curve is $\frac{u^*}{\kappa}$ and intercept is $-\frac{u^*}{\kappa}\ln(C)$. The shear velocity for each velocity profile can be calculated from the slope of the fitted linear regression curve.

The roughness function is a measure of how much a velocity profile (of a wall with different roughness geometries and suction velocities) is shifted downwards from a smooth wall velocity profile in a semi-log plot. The roughness function, ΔB, is a function of wire width, contour height, and slot velocity [i.e., $\Delta B = f\ (h,\ w,\ V_s)$]. The roughness function, ΔB, was obtained for each velocity profile by determining its downward shift from the smooth wall velocity profile. The log-law constant, B, (equal to 5.6)[17] and the roughness function, ΔB, are added together to define a new log-law constant B'. Figure 10 shows the function, B', for all contour heights, wire widths, and flow velocities tested. The figure indicates that B' increases with the contour height and decreases with the wire width. Furthermore, the results shown in this figure suggests that the velocity profile is the same for the wire geometries with similar ratios of the contour height to wire width (contour slope). This is industrially-significant, because it helps to resolve the debate on whether comparisons between differ-

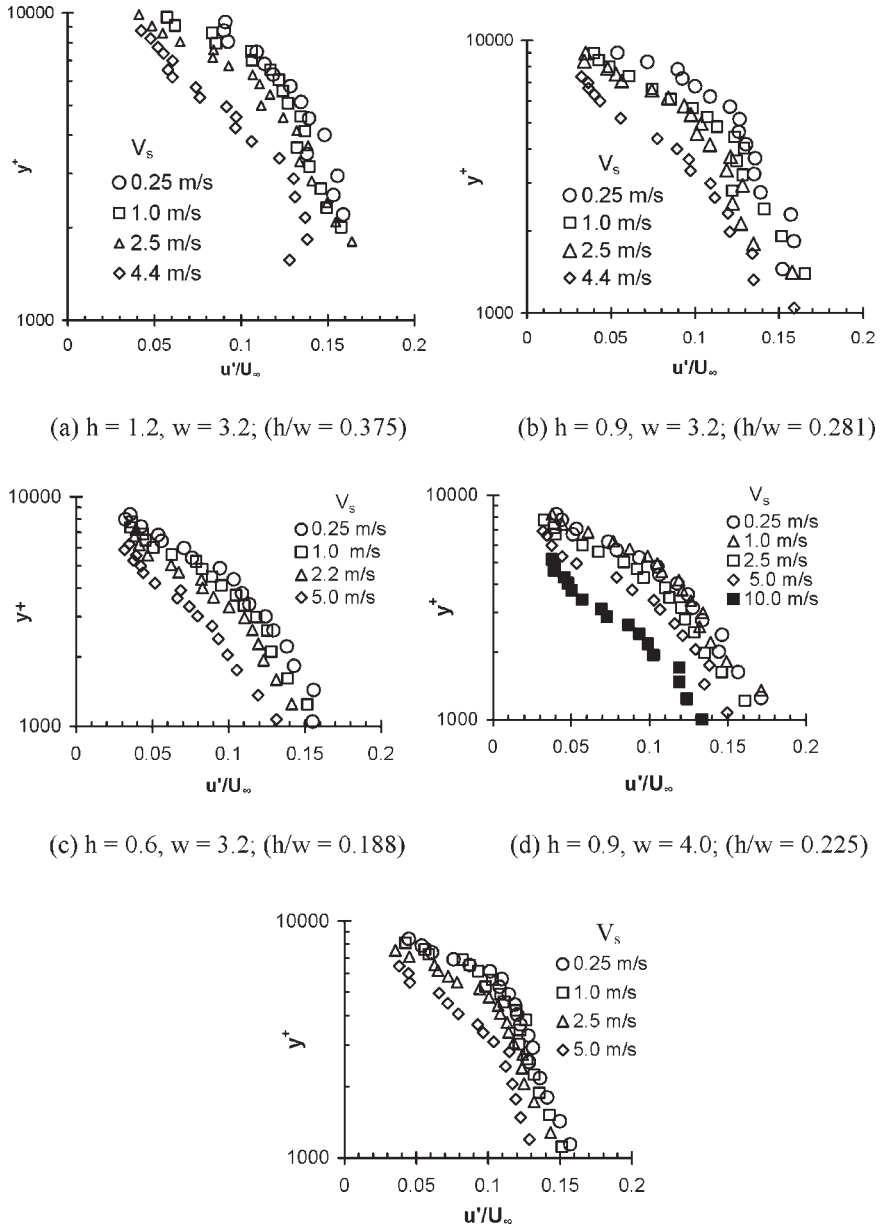

Figure 9. Effect of wall suction on the wall normal distribution of the stream-wise velocity fluctuations.

ent contours should be made on the basis of contour height or angle. As slot velocity increases, the roughness decreases. The effect of aperture geometry at high slot velocities is less than at low slot velocities. A correlation for the data shown in Figure 10 was developed and is given by Eq. 11.

$$B' = -20.96\left(\frac{h}{w}\right)^{0.62}\left(\frac{V_s}{U_\infty}\right) + 29.39\left(\frac{h}{w}\right)^{0.37} \quad (R^2 = 0.94) \tag{11}$$

where $B' = (-B + \Delta B)$

Figure 11 shows the relation between the shear velocity and B' for all the contour geometries and slot velocities tested. It indicates that the shear velocity varies linearly with B' as indicated by the correlation given by Eq. 12.

$$\frac{u^*}{U_\infty} = 0.005617B' \quad (R^2 = 0.937) \tag{12}$$

These correlations can be used to calculate the near-wall mean velocity for a range of conditions. However, their application is limited to the range of variables tested, that is, between 0.375 and 0.188 for h/w, and $V_s/U_\infty = 0.025 - 1.0$. One application could be to minimize the computation

required in CFD modeling of the flow through slots in pulp screens where this correlation can be implemented for ΔB in the log-law region. The correlation for shear velocity also enables the prediction of wall shear stress on the cylinder for a wide range of design and operating conditions. The wall shear stress on the cylinder can be one of the key parameters in determining the power consumption of the rotor.

Summary and Conclusions

The mean and rms fluctuations of stream-wise velocity profiles above a contoured surface in a steady cross flow with a series of flow bifurcations, similar to that in an idealized pulp pressure screen, were experimentally determined for various contour geometries and flow velocities. Velocity profiles were shown to be log-linear and a function of contour height, wire width, slot velocity, and cross-flow velocity. The local velocity decreased with the increasing contour height and decreasing wire width. Wires with similar ratios of contour height and wire width had similar profiles. Local velocity near the wall increased as slot velocity increased, and the boundary layer was pulled through the apertures. A correlation for mean velocity was determined for all the variables tested. The correlation can be used to estimate the wall shear stress on the cylinder within the range of tested variables. The stream-wise rms velocity fluctuations profile in the cross flow direction was also determined. The near-wall stream-wise velocity fluctuations were a strong function of the contour geometry and slot velocity. The maximum stream-wise velocity fluctuations near the wall was shown to increase with the contour height and decrease with the wire width. The maximum stream-wise velocity fluctuations decreased with the increasing slot velocity.

Acknowledgments

Financial support of NSERC is gratefully acknowledged.

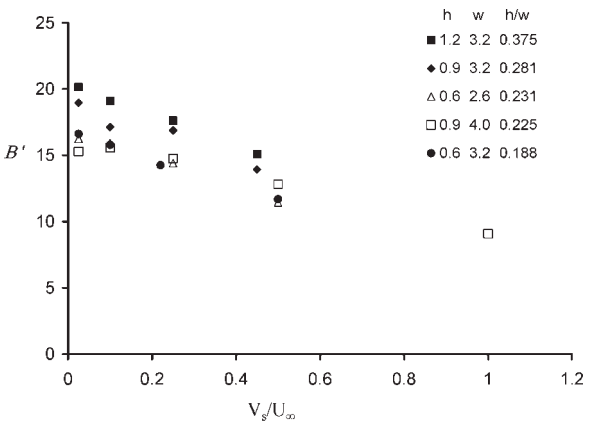

Figure 10. Effect of contour height and wire width on B' for varying slot velocities.

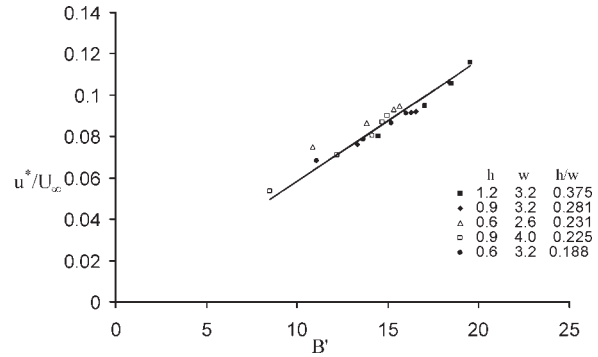

Figure 11. Relation between shear velocity and B' for different contour geometries and various slot velocities.

Notation

Symbols

B = a constant in log-law for smooth wall
B' = a modified constant in log-law for a rough wall with suction $(-B + \Delta B)$
ΔB = roughness function
$e1$ = unit vector
h = height of the contour, m
k = roughness height, m
k_s^+ = non-dimensional roughness height
n = total number of particles measured at a single point
Re = Reynolds number
s = slot width, mm
u^+ = nondimensional stream-wise velocity (u/u^*)
U_∞ = mean cross-flow velocity, m s^{-1}
U' = fluctuating component of x-velocity, m.s^{-1}
u^* = shear velocity ($\sqrt{\tau_w/\rho}$), m s^{-1}
$\mathbf{u}$ = instantaneous velocity vector of seeding particles, m s^{-1}
$\mathbf{u}_i$ = instantaneous velocity of the i^{th} particle, m s^{-1}
v = mean velocity normal to wall, m s^{-1}
V_s = mean slot velocity, m s^{-1}
u = local cross-flow velocity, m s^{-1}
V_w = wall suction velocity, m s^{-1}
$\frac{u'}{U_\infty}$ = normalized stream-wise velocity fluctuations
y' = distance from the top of roughness element, m
y = distance from wall, m
y^+ = nondimensional distance from wall ($y.u^*/\nu$)
w = width of the wire, m

Greek letters

κ = Karman constant
ν = kinematic viscosity (=0.6966 × *10^6 at 37°C), m^2 s^{-1}
ρ = density of fluid, kg m^{-3}
τ_w = wall shear stress, N m^{-2}

Literature Cited

1. Feng M, Gonzalez J, Olson JA, Ollivier-Gooch C, Gooding RW. Numerical simulation and experimental measurement of pressure pulses produced by a pulp screen foil rotor. *J Fluids Eng.* 2005;127:347–357.
2. Smook GA. *Handbook for Pulp & Paper Technologists*, 3rd ed. Vancouver: Angus-Wilde, 2002.
3. Gooding RW. M.A. Sc. Thesis. The Passage of Fibres Through Slots in Pulp Screening. University of British Columbia, Canada, 1986.
4. Gooding RW. Ph. D. Thesis. Flow Resistance of Screen Plate Apertures. University of British Columbia, Canada, 1996.
5. Kumar A. Ph.D. Thesis. Passage of Fibres Through Screen Apertures. University of British Columbia, Canada, 1991.

6. Olson JA. PhD Thesis. The Effect of Fibre Length on Passage Through a Single Screen Aperture. University of British Columbia, Canada, 1996.
7. Dong S. PhD Thesis. Modeling Fiber Motion in Pulp and Paper Equipment. University of British Columbia, Canada, 2002.
8. Halonen L, Ljokkoi R. Improved screening concepts. In: Proceedings of the TAPPI Pulping Conference, Seattle, USA, 1989:61–66.
9. Julien Saint Amand F, Perrin B. Fundamentals of screening: experimental approach and modeling. In: Proceedings of the TAPPI Pulping Conference, Montreal, 1998:1019–1031.
10. White FM. *Viscous Fluid Flow*, 2nd ed. New York: McGraw-Hill, 1991:411–414.
11. Thomas ASW, Cornelius KC. Investigation of laminar boundary layer suction in a slot. *AIAA J*. 1981;20:790–796.
12. Sano M, Hirayama M. Turbulent boundary layers with injection and suction through a slit, *JSME*. 1985;28:807–814.
13. Antonia RA, Zhu Y, Sokolov M. Effect of concentrated wall suction on a turbulent boundary layer. *Phys Fluids*. 1995;7:2465–2474.
14. Yoshioka S, Fransson JHM, Alfredsson PH. Free stream turbulence induced disturbances in boundary layers with wall suction. *Phys Fluids*. 2004;16:3530–3539.
15. Nikuradse J. Stroemungsgesetze in rauhen rohren. *VDI-Forsch. 361 (English translation: Laws of flow in rough pipes. NACA TM 1292)* 1950.
16. Zanoun E, Durst F, Nagib H. Evaluating the law of the wall in two-dimensional fully developed channel flows. *Phys Fluids*. 2003;15:3079–3089.
17. Shockling MA, Allen JJ, Smits AJ. Roughness effects in turbulent pipe flow. *J Fluid Mech*. 2006;564:267–285.
18. Patel VC, Yoon JY. Application of turbulence models to separated flow over rough surfaces. *J Fluids Eng*. 1995;117:234–241.
19. Simpson RL. A generalized correlation of roughness density effects on the turbulent boundary layer. *AIAA J*. 1973;11:242–244.
20. Schlichting H. *Boundary Layer Theory*, 6th ed. New York: McGraw-Hill, 1979.
21. Stevenson TN. Report 166, A law of the wall for turbulent boundary layers with suction or injection, Cranfield College of Aeronautics, Cranfield, UK, 1963.
22. Patel VC. Perspective: flow at high Reynolds number and over rough surfaces- Achilles heal of CFD. *ASME J. Fluids Eng*. 1998;120:434–444.
23. Lakehal D. Computation of turbulent shear flows over rough-walled circular cylinders. *J Wind Eng Ind Aerod*. 1999;80:47–68.
24. Gregoire G, Favre-Marinet M, Julien-Saint-Amand F. Modeling of turbulent fluid flow over a rough wall with or with out suction. *J Fluids Eng*. 2003;125:636–642.
25. Gullichsen J, Harkonen EJ. Medium consistency technology I: fundamental data." *Tappi J*. 1981;64:69–71.
26. Durst F, Melling A, Whitelaw JH. *Principles and Practice of Laser-Doppler Anemometry*. New York: Acad. Press, 1981.
27. Lissenburg RCD, Hinze JO, Leijdens H. An experimental investigation of the effect of a constriction on turbulent pipe flow. *Appl Sci Res*. 1975;31:343–362.
28. Deissler RG. Analysis of turbulent heat transfer and flow in the entrance regions of smooth passages. NASA Glenn Research Center, NACA TN 3016, 1953.
29. Coles DE, Hirst EA. Proceedings Computation of Turbulent Boundary Layers-1968 AFOSRIFP Stanford Conference, Vol. 2. Stnaford, Calif: Stanfird Univ, 1968.
30. Wei T, Schmidt R, McMurtry P. Comment on the Clauser chart method for determining the friction velocity. *Exp Fluids*. 2005;38: 695–699.
31. Kendall A, Koochesfahani M. A method for estimating wall friction in turbulent boundary layers. In: 25th AIAA Aerodynamic Measurement Technology and Ground Testing conference. San Francisco, CA, USA. 5–8 June 2006.
32. Spalding DB. A single formula for the law of the wall. *J Appl Mech Trans ASME*, Series E., 1961;83:455.
33. Bakkena OM, Krogstad P-A, Ashrafian A, Anderssond HI. Reynolds number effects in the outer layer of the turbulent flow in a channel with rough wall. *Phys Fluids*. 2005;17:065101–065116.

Manuscript received Sept. 6, 2007, and revision received May 7, 2008.